G4941K substitution in the pore-lining S6 helix of the skeletal muscle ryanodine receptor increases RyR1 sensitivity to cytosolic and luminal Ca^{2+}

Received for publication, June 20, 2017, and in revised form, December 18, 2017 Published, Papers in Press, December 18, 2017, DOI 10.1074/jbc.M117.803247

Le Xu[1], **David D. Mowrey**[1], **Venkat R. Chirasani, Ying Wang, Daniel A. Pasek, Nikolay V. Dokholyan**[2], **and Gerhard Meissner**[3]

From the Department of Biochemistry and Biophysics, University of North Carolina, Chapel Hill, North Carolina 27599

Edited by Roger J. Colbran

The ryanodine receptor ion channel RyR1 is present in skeletal muscle and has a large cytoplasmic N-terminal domain and smaller C-terminal pore-forming domain comprising six transmembrane helices, a pore helix, and a selectivity filter. The RyR1 S6 pore-lining helix has two conserved glycines, Gly-4934 and Gly-4941, that facilitate RyR1 channel gating by providing S6 flexibility and minimizing amino acid clashes. Here, we report that substitution of Gly-4941 with Asp or Lys results in functional channels as indicated by caffeine-induced Ca^{2+} release response in HEK293 cells, whereas a low response of the corresponding Gly-4934 variants suggested loss of function. Following purification, the RyR1 mutants G4934D, G4934K, and G4941D did not noticeably conduct Ca^{2+} in single-channel measurements. Gly-4941 replacement with Lys resulted in channels having reduced K^+ conductance and reduced selectivity for Ca^{2+} compared with wildtype. RyR1-G4941K did not fully close at nanomolar cytosolic Ca^{2+} concentrations and nearly fully opened at 2 μM cytosolic or sarcoplasmic reticulum luminal Ca^{2+}, and Ca^{2+}- and voltage-dependent regulation of RyR1-G4941K mutant channels was demonstrated. Computational methods and single-channel recordings indicated that the open G4941K variant results in the formation of a salt bridge to Asp-4938. In contrast, wildtype RyR1 was closed and not activated by luminal Ca^{2+} at low cytosolic Ca^{2+} levels. A model suggested that luminal Ca^{2+} activates RyR1 by accessing a recently identified cytosolic Ca^{2+}-binding site in the open channel as the Ca^{2+} ions pass through the pore.

The skeletal muscle ryanodine receptor ion channel (RyR1) is a 2,200-kDa homotetrameric ion channel that releases Ca^{2+} ions from an intracellular Ca^{2+} store, the sarcoplasmic reticulum (SR)[4] (1–5). The large RyR1 cytoplasmic N-terminal "foot" structure forms the site of regulation by multiple factors that include Ca^{2+}, Mg^{2+}, ATP, and *in vitro* ligands such as ryanodine and caffeine. The C-terminal transmembrane domain forms a pore in the SR membrane that conducts monovalent and divalent cations (~800 pS with 250 mM K^+ as conducting ion, ~150 pS with 50 mM Ca^{2+}) but is selective for divalent cations (permeability ratio of Ca^{2+}/K^+ ~7:1). Mutations in RyR1 give rise to central core disease and malignant hyperthermia muscle diseases (6). Many of the naturally occurring central core disease mutations are in the C-terminal pore-forming region and impair RyR1 activity and ion conductance.

RyR1 has a pore structure characteristic of the voltage-gated ion channel family (7–12). The RyR1 pore-forming region has an inner S6 helix, a pore helix, and a selectivity filter GGGIGDE motif (Fig. 1). Mutagenesis and single-channel measurements showed that negatively charged luminal residues Asp-4899 and Glu-4900 and the cytosolic residues Asp-4938, Glu-4942, and Asp-4945 in the pore-lining S6 helix impact RyR1 ion permeation and selectivity (13, 14). The RyR1 S6 pore-lining helix has also two conserved glycines, Gly-4934 and Gly-4941, whose replacement with uncharged residues with an increased side-chain volume altered RyR1 channel gating and ion permeation (15). High-resolution cryoelectron microscopy (cryo-EM) using open RyR1 (Fig. 1) and closed RyR1 (16) and cardiac muscle RyR2 isoforms (17) provided structural insights in the mechanisms of channel opening and closing. Binding sites for channel activators Ca^{2+}, ATP, and caffeine were identified (16). It was also shown that the RyR2 pore constriction site of Ile-4868 in the closed state is shifted to Gln-4864 in the open state (corresponding to Ile-4937 and Gln-4933 in RyR1, respectively) (17). Ion-pulling simulations that generated an open-channel conformation of RyR1 (18) from the 3.8-Å closed state of RyR1 (7) also showed that the pore constriction site was shifted from Ile-4937 in the closed channel to Gln-4933 in the open channel.

The premise of this study was that Gly-4934 and Gly-4941 have critical roles in the ion permeation and Ca^{2+} regulation of RyR1. We addressed this by replacing the two glycines with two oppositely charged residues, aspartic acid and lysine. The results indicate that RyR1-G4934D, G4934K, and G4941D mutants were not gated by Ca^{2+}, did not conduct Ca^{2+}, and had reduced K^+ conductances in single-channel measurements. In contrast to the closed wildtype (WT) channel, a K^+-conducting RyR1-G4941K mutant channel was recorded at nanomolar Ca^{2+} concentrations. The mutant channel was

This work was supported by National Institutes of Health Grant AR018687. The authors declare that they have no conflicts of interest with the contents of this article. The content is solely the responsibility of the authors and does not necessarily represent the official views of the National Institutes of Health.

[1] Both authors contributed equally to this work.
[2] To whom correspondence may be addressed. Tel.: 919-843-2513; E-mail: dokh@unc.edu.
[3] To whom correspondence may be addressed. Tel.: 919-966-5021; E-mail: meissner@med.unc.edu.

[4] The abbreviations used are: SR, sarcoplasmic reticulum; pS, picosiemens; PDB, Protein Data Bank; MD, molecular dynamics; APBS, Adaptive Poisson-Boltzmann Solver.

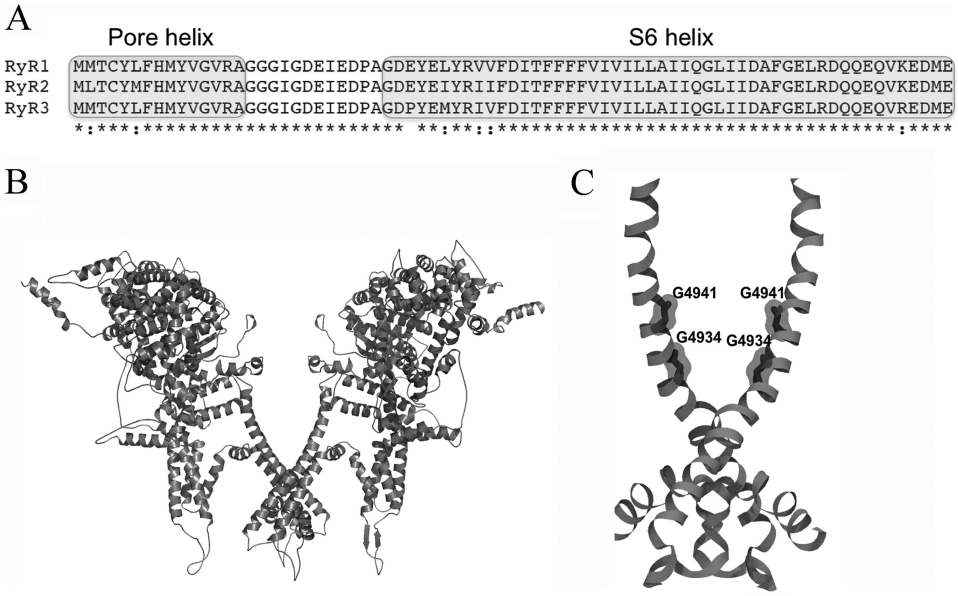

Figure 1. Alignment of RyR pore sequences and RyR1 structures. *A,* shown are the amino acid sequences of the pore region of rabbit RyR1, RyR2, and RyR3. *B,* open RyR1 channel structure (PDB code 5tal). *C,* pore structure of RyR1 (PDB code 5tal). For clarity, *B* and *C* show only two of the four RyR1 subunits.

nearly fully opened by SR luminal Ca^{2+} in a voltage-dependent manner, which suggested that luminal Ca^{2+} activated RyR1-G4941K by accessing a cytosolic Ca^{2+}-binding site. Computational methods suggested that RyR1-G4941K formed a salt bridge with Asp-4938. Single-channel measurements of RyR1-G4941K/D4938N and RyR1-G4941K/D4945N mutants validated the computational predictions.

Results

Expression and functional properties of RyR1-Gly-4934 and RyR1-Gly-4941 mutants

To assess the functional role of two conserved glycines in the S6 pore-lining helix in RyR1 gating and ion permeation, Gly-4934 and Gly-4941 were mutated to negatively charged aspartic acid and positively charged lysine. RyR1 mutant protein expression levels in HEK293 cells ranged from ~50 to 100% of WT (Table 1). In initial experiments, expression of functional channels was studied using two assays. A cellular Ca^{2+} release assay indicated the number of HEK293 cells that expressed Ca^{2+}-conducting WT and mutant channels, using the Ca^{2+}-releasing drug caffeine. Retention of function in membrane isolates was determined in an *in vitro* ligand-binding assay using [^{3}H]ryanodine, a plant alkaloid commonly used to assess RyR activity and content (19). Caffeine-induced Ca^{2+} release was observed in 30–50% of HEK293 cells that expressed WT-RyR1 (Fig. 2). Cells expressing RyR1-G4934D or -G4934K showed a caffeine response near background levels, whereas replacement of Gly-4941 with aspartic acid or lysine showed a caffeine response similar to WT in ~75% of cells. This suggests a reduced number of HEK293 cells expressed caffeine-sensitive, Ca^{2+}-conducting mutant channels. The variable responses may have resulted from the non-homogeneous exposure to caffeine and removal of Ca^{2+} by cellular transport systems. The *in vitro* [^{3}H]ryanodine-binding assay in membrane isolates showed no binding for RyR1-G4934D to levels for RyR1-G4941K that exceeded WT (Table 1). This indicated variable levels of retention of function of the mutants compared with WT. Major differences in cellular caffeine-induced Ca^{2+} release response and [^{3}H]ryanodine binding in membrane isolates were observed for RyR1-G4934K and -G4941D. These may have resulted from RyR1-G4934K having a reduced sensitivity to caffeine and RyR1-G4941D having lost function during isolation or in the binding assay. An alternative possibility for reduced sensitivity to caffeine and loss of high-affinity [^{3}H]ryanodine binding but not Ca^{2+}-dependent channel activity is considered in single-channel measurements described below.

Single-channel measurements with WT- RyR1 and Gly-4934 and Gly-4941 mutants

Single channel measurements were performed with purified WT and mutant RyR1s to determine how mutagenesis of Gly-4934 and Gly-4941 affected channel gating and ion permeation. WT and mutant RyR1 channels were solubilized using the zwitterionic detergent CHAPS, purified on sucrose gradients, and reconstituted in proteoliposomes by removing the detergent by dialysis (20). In recording single channels, we took advantage of the finding that RyRs are Ca^{2+}-gated channels impermeant to Cl^- and conduct K^+ more efficiently than Ca^{2+}. The *upper left trace* in Fig. 3*A* shows a partially activated single WT-RyR1 channel recorded using 0.25 M KCl and 2 μM Ca^{2+} on both sides of the bilayer. K^+ conductance was 820 pS (Fig. 3*A*, *right panel*, and Table 1). Reduction to 0.1 μM cytosolic Ca^{2+} decreased channel open probability (P_o) to near zero (Fig. 3*A*, *2nd trace on left*, and Table 1). In the presence of 10 mM SR luminal Ca^{2+}, a Ca^{2+} current of −2.3 pA at 0 mV and reversal potential (E_{rev}) of 9.2 were obtained (Fig. 3*A*, *3rd trace, right panel*). Applying constant field theory, E_{rev} of 9.2 mV resulted in a permeability ratio of Ca^{2+} over K^+ (P_{Ca}/P_K) of 6.6 for WT (Table 1).

RyR1-G4934D and G4934K mutant channels were nearly fully open at 2 μM cytosolic Ca^{2+} (P_o >0.9), whereas RyR1-G4941D had P_o 3–4-fold that of WT (Fig. 3, *B–D*, *top traces on left*, and Table 1). Reduction from 2 to 0.1 μM cytosolic Ca^{2+}

Table 1
Single channel measurements with wildtype and mutant RyR1s
The following abbreviations are used: Ry, ryanodine; ND, not determined. Caffeine response indicates the number of HEK293 cells showing a caffeine-induced Ca^{2+} response normalized to WT. Single-channel data of mutant channels not conducting Ca^{2+} were excluded from the statistical analysis. Single-channel open probabilities (P_o) and K^+ conductances were determined with 2 μM Ca^{2+} in the *trans* (SR luminal) lipid bilayer chamber. Ca^{2+} currents were determined at 0 mV.

	Intensity on immunoblots	Caffeine response	B_{max} of [^{3}H]Ry binding	P_o (2 μM calcium)	P_o (0.1 μM calcium)	γ_K^+	I_{Ca} (+10 mM calcium trans)	P_{Ca}/P_K
	% WT	*% WT*	*% WT*			*pS*	*pA*	
WT-RyR1	100	100	100	0.13 ± 0.04(9)	0.01 ± 0.01(5)	820 ± 3(9)	−2.3 ± 0.1(5)	6.6 ± 0.1(5)
G4934D	51.4 ± 12.8(5)	2.0 ± 1.4(4)^{a,b}	0 ± 0(6)^{a,b,c}	0.91 ± 0.05(13)	0.95 ± 0.04(5)	519 ± 45(15)	−0.1 ± 0.1(11)	ND
G4934K	80.0 ± 24.9(5)	2.6 ± 1.3(4)^{a,b}	24.8 ± 6.0(9)^{a,b,c}	0.99 ± 0.10(15)	0.57 ± 0.17(7)	304 ± 30(20)	−0.1 ± 0.1(10)	ND
G4941D	106.2 ± 28.7(6)	84.0 ± 30.0(4)	5.3 ± 2.2(6)^{a,b,c}	0.48 ± 0.18(7)	0.51 ± 0.11(7)	413 ± 79(9)	−0.1 ± 0.1(7)	ND
G4941K	80.6 ± 18.7(5)	72.9 ± 19.2(4)	130.5 ± 14.9(15)^{d}	0.89 ± 0.04(14)^{a}	0.56 ± 0.10(9)^{a}	364 ± 5(10)^{a,c,d}	−0.6 ± 0.1(7)^{a,d}	2.1 ± 0.1(7)^{a,d}
G4941 M	115.6 ± 11.2(5)	63.5 ± 11.2(4)	37.8 ± 9.2(10)^{a,b,c}	0.15 ± 0.05(9)^{b}	0.01 ± 0.01(9)^{b}	773 ± 3(9)^{b,c}	−2.0 ± 0.1(7)^{b}	6.0 ± 0.1(6)^{b,c}
D4938N	84.1 ± 29.3(4)	49.9 ± 11.6(5)	128.3 ± 14.3(8)^{d}	0.13 ± 0.04(15)^{b}	0.01 ± 0.01(3)^{b}	520 ± 6(9)^{a,b,d,e}	−0.8 ± 0.1(4)^{a,d,e}	3.3 ± 0.2(4)^{a,d,e}
G4941K/D4938N	97.5 ± 5.2(5)	115.3 ± 15.2(4)^{c,d}	135.0 ± 23.1(7)^{d}	0.13 ± 0.05(4)^{b}	0.22 ± 0.14(4)	264 ± 78(4)^{a,b,c,d}	−0.6 ± 0.1(4)^{a,d}	<1 (4)^{a,b,c,d}
D4945N	61.7 ± 33.6(4)	41.7 ± 3.6(5)	50.9 ± 4.8(8)^{b,c}	0.06 ± 0.02(11)^{b}	0.01 ± 0.01(3)^{b}	737 ± 11(6)^{a,b,c,e}	−2.0 ± 0.2(5)^{b,c,e}	6.5 ± 0.6(5)^{b,e}
G4941K/D4945N	48.2 ± 12.6(5)	40.9 ± 10.4(4)	57.6 ± 9.1(7)^{b,c}	0.99 ± 0.01(5)^{a,c,d}	0.99 ± 0.01(5)^{a}	183 ± 3(5)^{a,b,c,d}	−0.5 ± 0.1(4)^{a,d}	1.0 ± 0.2(5)^{a,d}

[a] $p < 0.05$ compared with WT.
[b] $p < 0.05$ compared with G4941K.
[c] $p < 0.05$ as compared with D4938N.
[d] $p < 0.05$ as compared with D4945N by analysis of variance.
[e] Data are from Ref. 14.

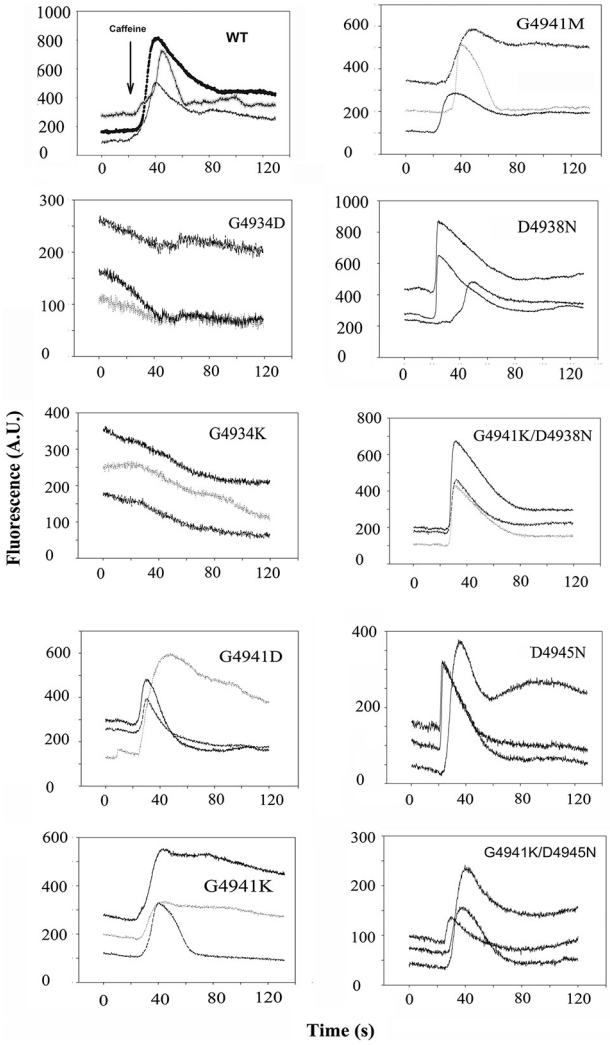

Figure 2. Caffeine-induced Ca^{2+} release in HEK293 cells expressing WT and mutant RyR1s. Ca^{2+} transients were determined in Ca^{2+}-free Krebs Ringers Henseleit bath solution as changes of Fluo-4 fluorescence (F/F_o) before and following the addition of ~8 mM caffeine to the bath solution. *Arrow* in *top left panel* indicates the position of caffeine addition to WT and mutant cells. Number of mutant cells showing a caffeine response were normalized to WT cells showing a caffeine response and are summarized in Table 1.

reduced P_o of RyR1-G4934K about 2-fold, whereas RyR1-G4934D and G4941D maintained a similar P_o at 2 and 0.1 μM cytosolic Ca^{2+}. The three RyR1-G4934K, G4934D, and G4941D mutants exhibited a reduced K^+ conductance and did not conduct Ca^{2+}. We considered the possibility that exposure to detergent during purification caused loss of function. However, RyR1-G4934D, G4934K, and G4941D also had a reduced K^+ conductance and did not conduct Ca^{2+} when membrane fractions isolated from HEK293 cells were fused with lipid bilayers (data not shown). This suggested that RyR1-G4934D, G4934K, and G4941D mutations had a major impact on channel structure and impaired ion conductances in single-channel measurements.

RyR1-G4941K conducted Ca^{2+} and had a reduced K^+ conductance of 364 pS between ±40 mV compared with 820 pS for WT with 0.25 M KCl on both sides of the bilayer (Fig. 3*E* and Table 1). Changes in KCl concentration indicated maximal K^+

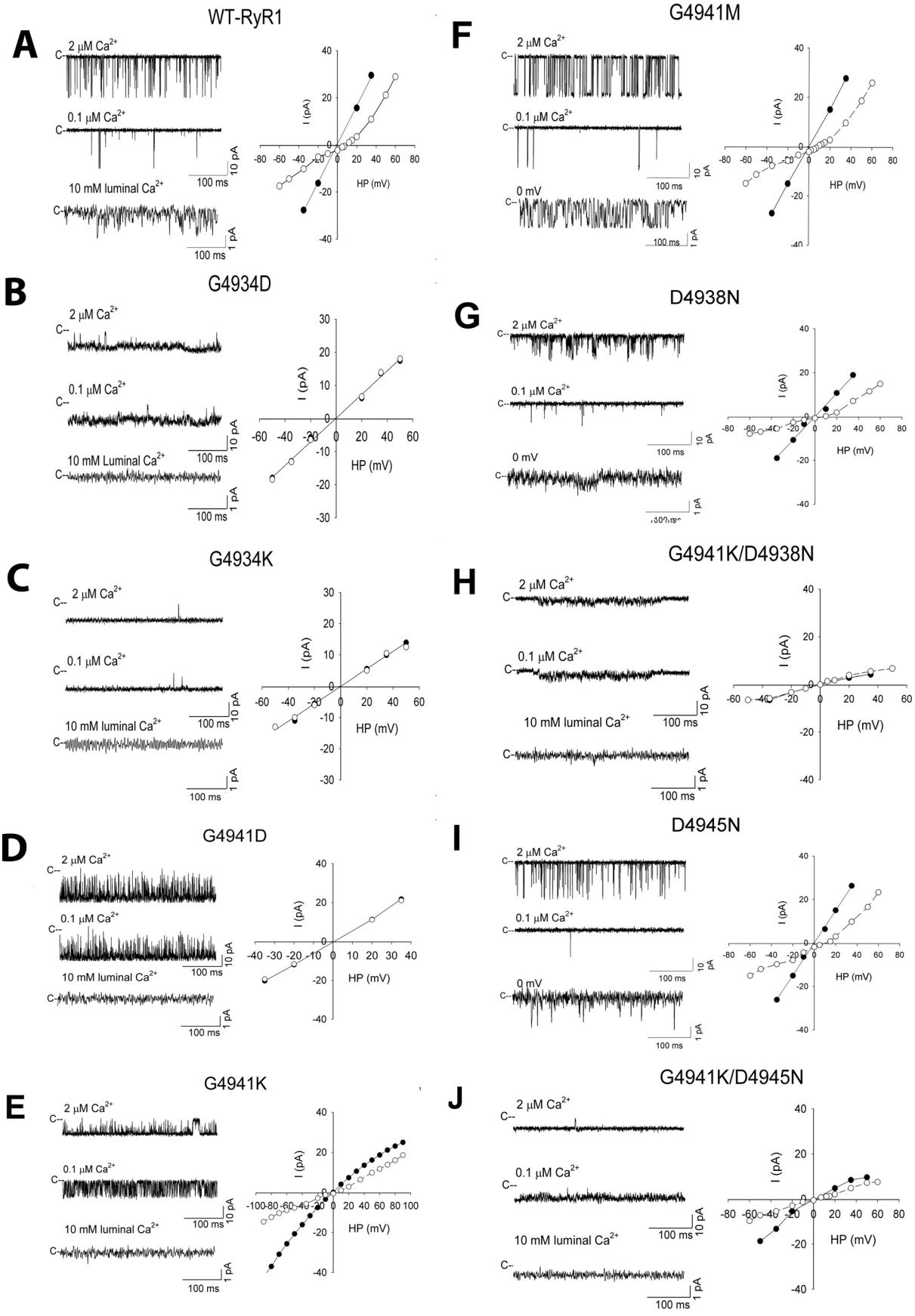

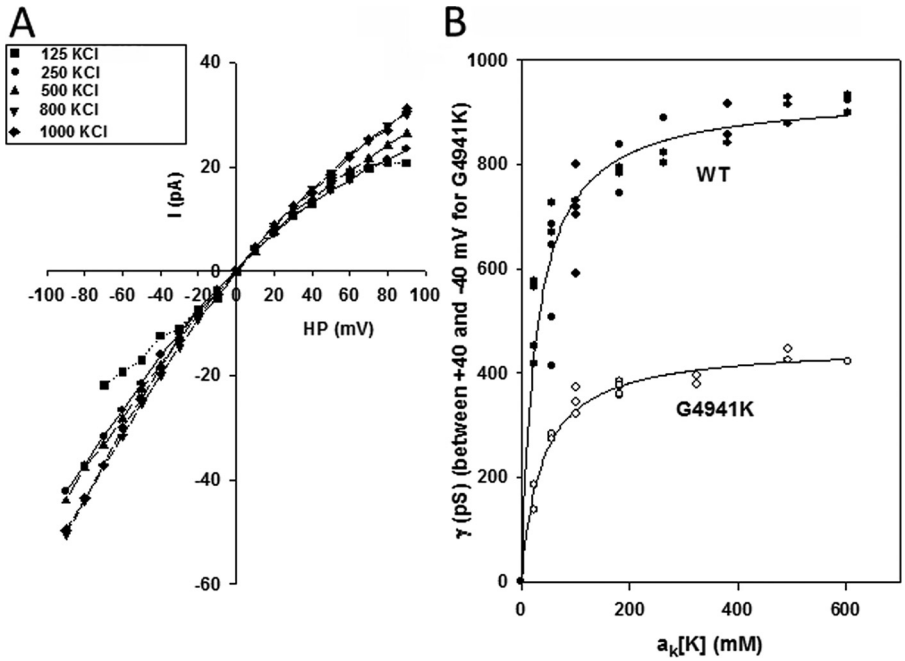

Figure 4. Conductances as a function of K^+ activity. *A,* representative current voltage relations of G4941K at indicated symmetrical KCl concentrations. *B,* relationships between WT (●) and G4941K (○) conductances and K^+ activities give K_D = 28 mM and γ_{max} = 943 pS for WT and K_D = 38 mM and y_{max} = 453 pS for G4941K, using equation $\gamma = \gamma_{max}(1 + K_D/a_K[K])^{-1}$.

conductances for WT-RyR1 and RyR1-G4941K near 600 mosM K^+ (Fig. 4). Maximal conductances and apparent K_D values were 453 pS and 38 mM for G4941K *versus* 943 pS and 28 mM for WT. In the presence of 10 mM luminal Ca^{2+}, the Ca^{2+} current (−0.6 pA *versus* −2.3 pA for WT at 0 mV) and permeability ratio of Ca^{2+} over K^+ (P_{Ca}/P_K = 2.1 *versus* 6.6 for WT) were greatly reduced (Table 1).

Channel open probability of RyR1-G4941K was elevated at 2 μM cytosolic Ca^{2+} (0.89 *versus* 0.13 for WT) and 0.1 μM Ca^{2+} (0.56 *versus* 0.01 for WT) (Fig. 3*E*, Table 1). At 2 μM Ca^{2+} in the bath solution, the RyR1-G4941K mutation increased the duration of open events (34.6 ms *versus* 0.47 ms for WT) and decreased the duration of the closed events (0.32 ms *versus* 6.5 ms for WT) (Table 2). The results suggest that RyR1-G4941K exhibited altered Ca^{2+}-dependent gating and reduced ion conductances compared with WT.

As a control, RyR1-G4941M was analyzed with methionine having a side-chain volume comparable with lysine. RyR1-G4941M exhibited caffeine-induced Ca^{2+} release in HEK293 cells (Fig. 2) and bound [^{3}H]ryanodine in an *in vitro* ligand-binding assay, albeit at reduced levels compared with WT (Table 1). Single-channel measurements showed that replacement of a positively charged residue in G4941K with methionine with a comparable side-chain volume but uncharged side chain resulted in channel open probability, K^+ conductance, and permeability ratios of Ca^{2+} over K^+ close to WT (Fig. 3*F* and Table 1).

Activation of RyR1-G4941K by 2 μM cytosolic or 2 μM luminal Ca^{2+}

Dependence of WT-RyR1 and RyR1-G4941K single-channel activities by 2 μM cytosolic or 2 μM luminal Ca^{2+} was determined at −35 mV membrane potential, which promoted the movement of luminal Ca^{2+} to the *cis* cytosolic side of the bilayer (Fig. 5). In the presence of 0.01 μM cytosolic and luminal Ca^{2+}, WT P_o was essentially 0, and G4941K P_o was 0.13. An increase in luminal or cytosolic Ca^{2+} to 2 μM Ca^{2+} nearly fully activated RyR1-G4941K (P_o = 0.86 and 0.98, respectively), whereas WT was incompletely activated by 2 μM cytosolic Ca^{2+} (P_o = 0.16). The results indicate that in contrast to WT, (i) RyR1-G4941K had a P_o >0.1 at low cytosolic and luminal Ca^{2+}, which indicated Ca^{2+}-independent open channel state(s), and (ii) was nearly fully opened (P_o close to 1.0) by 2 μM luminal or 2 μM cytosolic Ca^{2+}.

Altered regulation of RyR1-G4941K by cytosolic Ca^{2+} in the presence of 2 μM luminal Ca^{2+}

In agreement with rapid $^{45}Ca^{2+}$ flux measurements of SR vesicles (21). WT-RyR1 channels were activated by micromolar cytosolic Ca^{2+} and inhibited by millimolar cytosolic Ca^{2+} at −35 mV (Fig. 6). Ca^{2+}-dependent regulation of G4941K differed in several respects from WT. G4941K had elevated open probability at 0.01 μM cytoplasmic Ca^{2+} in the presence of 2 μM luminal Ca^{2+}. G4941K was also nearly fully activated at 2 −100

Figure 3. Single-channel measurements of WT and mutant RyR1 channels. *Left panels* show representative single-channel currents at −35 mV (*upper* and *middle traces*) or 0 mV (*bottom traces*) as downward deflections from the closed states (*c*−). Channels were recorded in symmetrical 250 mM KCl, 20 mM KHEPES, pH 7.4, 2 μM Ca^{2+} bath solution (*upper traces*) and following the subsequent addition of EGTA to yield free cytosolic Ca^{2+} of 0.1 μM (*middle traces*) or the addition of 10 mM Ca^{2+} to the luminal chamber (*bottom traces*). *Right panels* show representative current voltage relationships in 250 mM symmetrical KCl (●) and after the addition of 10 mM luminal Ca^{2+} (○). Averaged P_o values and ion permeation properties are summarized in Table 1.

Table 2

Time analysis of wildtype and mutant RyR1s

Single channels were recorded at 2 μM cytosolic and 2 μM luminal Ca^{2+} were analyzed.

	P_o	No. of events/min	T_o	T_c
			ms	*ms*
WT-RyR1	0.12 ± 0.04(6)	13,242 ± 2776(6)	0.47 ± 0.06(6)	6.50 ± 2.60(6)
G4941K	0.96 ± 0.01(10)[a,b]	7651 ± 1828(10)	34.6 ± 17.9(10)	0.32 ± 0.03(10)[b]
G4941M	0.15 ± 0.06(7)[c]	8036 ± 1676(7)	0.93 ± 0.29(7)	8.90 ± 2.37(7)
D4938N	0.13 ± 0.04(14)[c]	16,829 ± 2445(14)	0.39 ± 0.05(14)	6.80 ± 3.30(14)[b]
G4941K/D4938N	0.13 ± 0.06(4)[c]	4291 ± 1193(4)	1.29 ± 0.19(4)	28.8 ± 15.3(4)
D4945N	0.05 ± 0.03(8)[c]	8237 ± 4044(8)	0.31 ± 0.02(8)	71.4 ± 34.6(8)[c]
G4941K/D4945N	0.99 ± 0.01(5))[a,b,d]	125 ± 76(5)[d]	2091 ± 1115(5)[a,b,c,d]	0.45 ± 0.11(5)[b]

[a] $p < 0.05$ compared with WT.
[b] $p < 0.05$ compared with D4945N by analysis of variance.
[c] $p < 0.05$ compared with G4941K.
[d] $p < 0.05$ compared with D4938N.

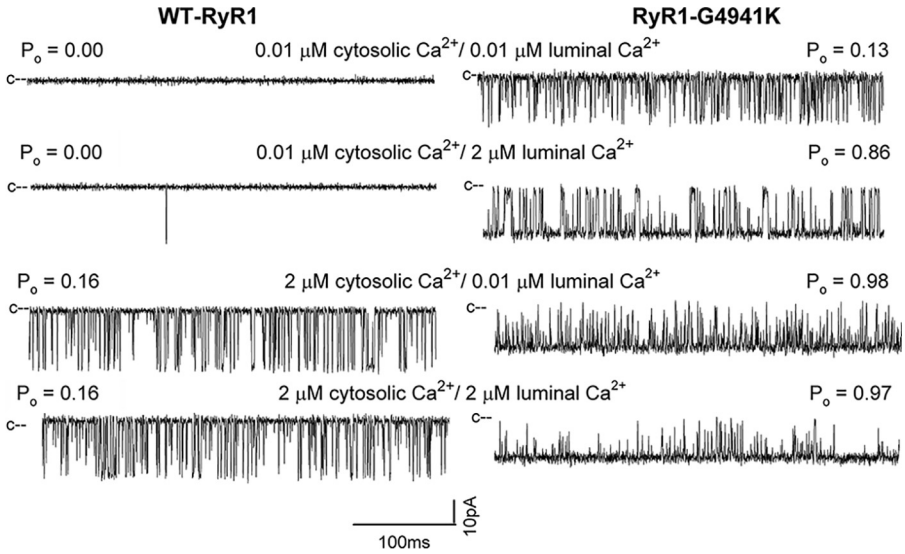

Figure 5. Effects of cytosolic and luminal Ca^{2+} on single-channel open probabilities of WT and G4941K mutant channels. Single-channel currents are shown at −35 mV as downward deflections from the closed states (*c*−) in symmetrical 250 mM KCl at indicated Ca^{2+} concentrations in luminal and cytosolic bilayer chambers.

μM cytosolic Ca^{2+} and displayed elevated activity at 10 mM cytosolic Ca^{2+} compared with WT.

RyR1-G4941K regulation by luminal Ca^{2+}

RyR1 has been reported to be regulated by luminal Ca^{2+} by binding to luminal channel sites (22) or cytosolic sites following passage of luminal Ca^{2+} through the open channel (23). To distinguish these mechanisms, dependence of channel open probability on the luminal Ca^{2+} concentration was probed at −35 and +35 mV (Fig. 7). Cytosolic Ca^{2+} was 0.01 or 2 μM. In WT at 0.01 cytosolic Ca^{2+}, an increase from 0.01 to 10 mM luminal Ca^{2+} did not increase the low P_o at −35 or +35 mV (Fig. 7*A*). At 2 μM cytosolic Ca^{2+}, an increase of luminal Ca^{2+} from 0.01 to 10 mM significantly decreased P_o at −35 mV but not at +35 mV. Regulation of RyR1-G4941K by luminal Ca^{2+} differed greatly from WT (Fig. 7*B*). At 2 μM cytosolic Ca^{2+}, RyR1-G4941K was fully activated at both membrane potentials at 0.01 μM to 10 mM luminal Ca^{2+} At 0.01 μM cytosolic Ca^{2+}, which kept the mutant channel open, luminal Ca^{2+} was more effective in increasing P_o at negative than positive membrane potentials. This suggested that luminal Ca^{2+} flowing through the channel accessed cytosolic Ca^{2+} activation sites in RyR1-G4941K. This was tested further by recording voltage dependence of RyR1-WT and -G4941K channel activities at 0.01 μM cytosolic Ca^{2+} and 0.01 or 2 μM luminal Ca^{2+} (Fig. 8). At 0.01 and 2 μM luminal Ca^{2+}, WT channels were closed, displaying no voltage-dependent activity. At 0.01 μM luminal Ca^{2+}, RyR1-G4941K displayed a weak voltage-dependent P_o at membrane potentials ranging from −80 to +80 mV. At 2 μM luminal Ca^{2+}, P_o was higher at negative than positive membrane potentials. Thus, a larger number of Ca^{2+} ions appeared to flow through the channel at negative than positive membrane potentials to activate RyR1-G4941K to a greater extent at negative potentials.

RyR1-WT and -G4941K activities in the presence of FKBP12 and in membrane isolates

We considered the possibility that elevated RyR1-G4941K channel open probability may result from the absence of FKBP12, a closely associated subunit of RyR1. Absence of FKBP12 in the WT-RyR1 macromolecular complex activates Ca^{2+} release from the SR and increases channel activity in lipid bilayers (24, 25). Proteoliposomes containing purified WT and RyR1-G4941K channels were therefore treated for 30 min with 5 μM FKBP12 before addition to the *cis* bilayer chamber. Treatment of WT and RyR1-G4941K with FKBP12 did not significantly affect P_o at 0.1 and 2 μM Ca^{2+} compared with channels recorded in the absence of FKBP12, respectively (Fig. 9, *A* and *B*). To increase

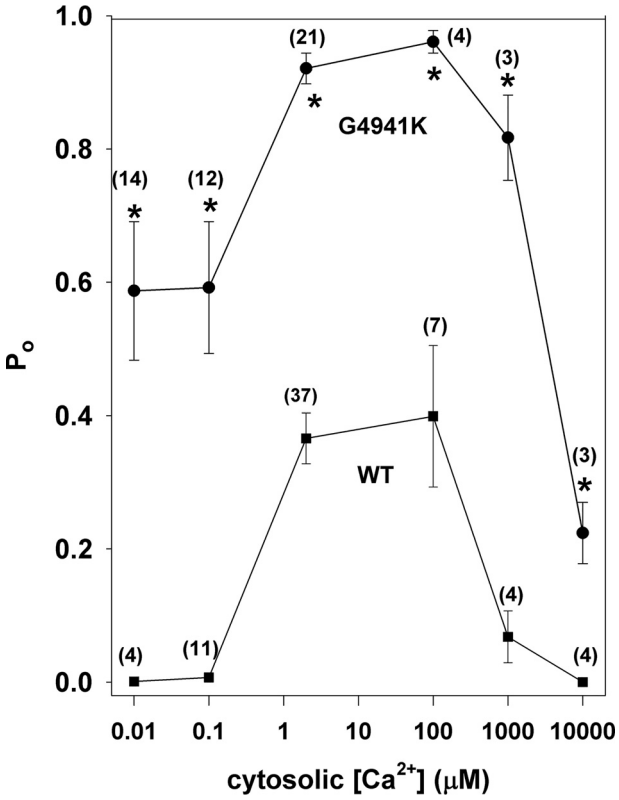

Figure 6. Effects of cytosolic Ca^{2+} on P_o of WT and G4941K mutant channels. Single-channel open probabilities of WT (■) and G4941K (●) were determined at −35 mV in symmetrical 250 mM KCl with 2 μM luminal Ca^{2+} and indicated cytosolic Ca^{2+} concentrations. Data are the mean ± S.E. of number of recordings in parenthesis. *, $p < 0.05$ compared with WT by Student's *t* test.

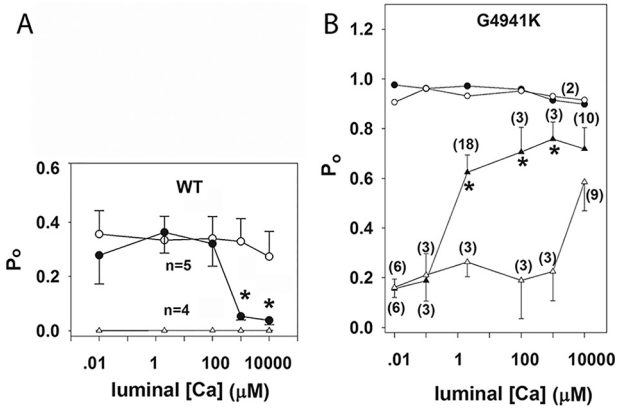

Figure 7. Effects of luminal Ca^{2+} on WT and G4941K mutant channel activities. Single open channel probabilities of WT (*A*) and G4941K (*B*) were determined at −35 mV (● and ▲) or +35 mV (○ and △) in symmetrical 250 mM KCl with 0.01 μM (△ and ▲) or 2 μM (○ and ●) cytosolic Ca^{2+} and indicated luminal Ca^{2+} concentrations. Data are the mean ± S.E. of indicated recordings. *, $p < 0.05$ compared with + 35 mV by Student's *t* test.

the probability of preserving normal function, experiments were also performed with channels that were not subjected to detergent treatment. Fig. 9, *A* and *B*, shows that RyR1-G4941K channels obtained using membrane preparations isolated from HEK293 cells maintained an elevated P_o at 0.1 and 2 μM cytosolic Ca^{2+} compared with WT, respectively. The results indicate that preincubation with FKBP12 and elimination of detergent treatment did not decrease the single-channel activities of RyR1-G4941K to those of WT.

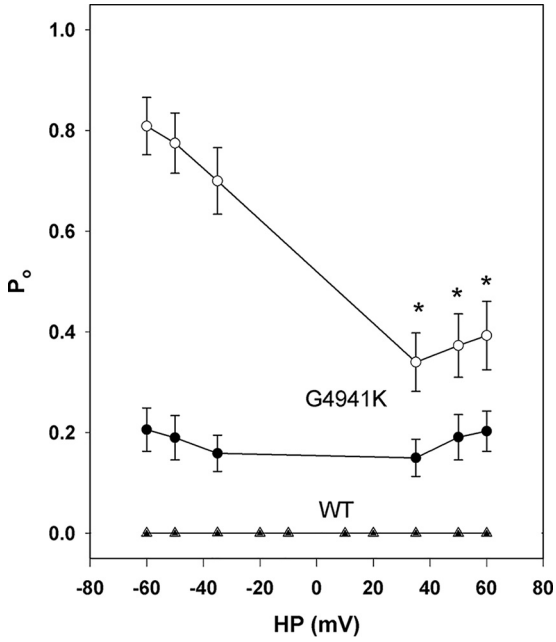

Figure 8. Effects of luminal Ca^{2+} and membrane potential on P_o of WT and G4941K mutant channel activities. Single-channel open probabilities of WT (△ and ▲) and G4941K (○ and ●) were determined in 250 mM symmetrical KCl at 0.01 μM (● and ▲) or 2 μM (○ and △) luminal Ca^{2+} and indicated membrane potentials. Cytosolic Ca^{2+} was 0.01 μM. Data are the mean ± S.E. of 4 (*WT*) and 7 (G4941K) recordings. *, $p < 0.05$ compared with corresponding negative voltages by Student's *t* test.

RyR1-G4941K interaction with RyR1-Asp-4938 and Asp-4945

Modeling revealed an interaction of RyR1-G4941K with Asp-4938 (Fig. 10, see under "Discussion"). The computational predictions were tested by performing single-channel measurements with RyR1-G4941K/D4938N and G4941K/D4945N double mutants. Their properties were compared with WT, RyR1-G4941K, and two previously studied single-site mutants (RyR1-D4938N and -D4945N) (Tables 1 and 2) (14). The two single-site (D4938N and D4945N) and double-site (G4941K/D4938N and G4941K/D4945N) mutants had cellular caffeine-induced Ca^{2+} release and bound [^{3}H]ryanodine that indicated function was retained (Fig. 2 and Table 1). In single-channel measurements, substitution of Asp-4938 with Asn in RyR1-D4938N and RyR1-G4941K/D4938 and Asp-4945 with Asn in RyR1–4941K/D4945 reduced K^+ conductances and Ca^{2+} currents at 0 mV (Fig. 3 and Table 1). In contrast, RyR1-D4945N maintained K^+ conductance and Ca^{2+} current close to WT–RyR1.

RyR1-D4938N, -D4945N, and -G4941K/D4938N had channel open probabilities comparable with WT-RyR1 at 2 μM cytosolic Ca^{2+} (Fig. 3 and Table 1). In contrast, RyR1-G4941K/D4945N maintained high P_o comparable with RyR1-G4941K (P_o ~1.0 *versus* 0.89). Significant differences were also obtained for the open and closed times (Table 2). Compared with the D4938N mutant, the mean open time of RyR1-G4941K/D4938N increased 4-fold ($p < 0.05$, Student's *t* test), and compared with G4941K, it decreased ~25-fold. Mean closed time of RyR1-G4941K/D4938N increased ~4-fold compared with WT-RyR1 and RyR1-D4938N ($p < 0.05$, Student's *t* test). The mean open time of RyR1-G4941K/D4945N increased ~4000-, ~60-, and 6,500-fold, respectively, compared with WT, RyR1-

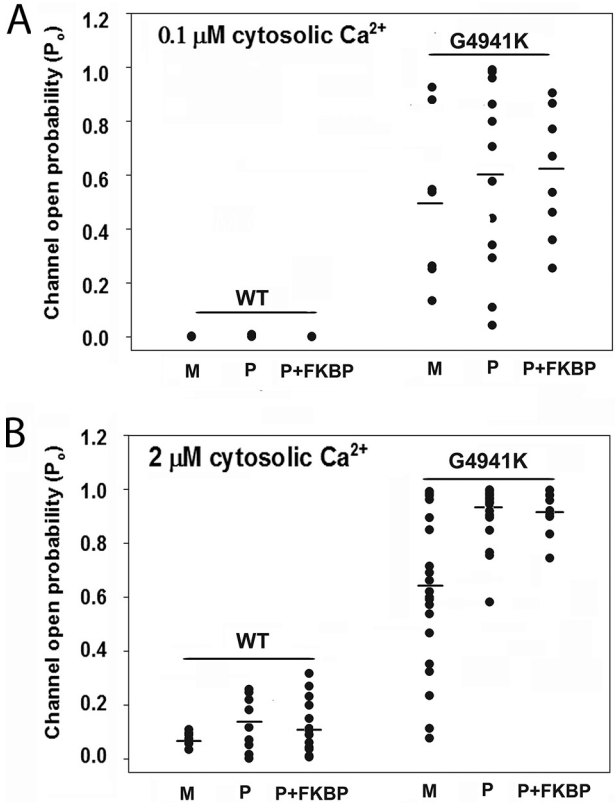

Figure 9. Effects of FKBP12 on purified WT and G4941K mutant channel open probabilities and fusing membrane fractions with lipid bilayers. Single open probabilities of WT and G4941K in 250 mM symmetrical KCl were determined at −35 mV. SR luminal Ca^{2+} was 2 μM. Single-channel open probabilities were at 0.1 μM (*A*) and 2 μM (*B*) cytosolic Ca^{2+} of WT and G4941K membrane isolates (*M*), purified WT, and G4941K mutant channels not incubated (*P*), and incubated with 5 μM FKBP12 for 30 min at 24 °C (*P+FKBP*). *Bars* show means of data.

G4941K, and D4945N. The mean closed time of RyR1-G4941K/D4945N decreased 14-fold compared with WT, was comparable with RyR1-G4941K, and decreased ~160-fold compared with RyR1-D4945N. The results suggest that attenuation of the G4941K interaction with Asp-4938 favors the closed state, whereas attenuation of the G4941K-D4945 interaction favors the open state.

Discussion

The principal finding of this study is that RyR1-G4941K exhibits a marked increase in the sensitivity of SR luminal Ca^{2+} regulation in single-channel recordings. The RyR1-G4941K mutant exhibited a caffeine-induced Ca^{2+} response in HEK293 cells and bound [^{3}H]ryanodine, but it had reduced Ca^{2+} over K^+ permeability ratio compared with WT. This was in contrast to the finding that RyR1-G4934D and -G4934K mutants lost caffeine-induced Ca^{2+} response in HEK293 cells, had a pronounced decrease in [^{3}H]ryanodine binding, and Ca^{2+} currents decreased to background levels. These findings suggest loss-of-function channels in HEK293 cells, membrane isolates, and single-channel measurements. By comparison, the G4941D mutation resulted in a more complex behavior. RyR1-G4941D responded to caffeine, which suggested the formation of a functional Ca^{2+}-conducting channel in HEK293 cells. However, [^{3}H]ryanodine binding was low, and Ca^{2+} currents decreased to background levels, which suggested loss of function on removal from HEK293 cells. The mutagenesis results support the modeling data described below that RyR1-G4941K forms a salt bridge to Asp-4938 and luminal Ca^{2+} accesses a recently identified Ca^{2+}-binding site in the open-channel conformation.

Our results suggest that the RyR1-G4941K mutant undergoes a structural change during extraction from HEK293 cells. The caffeine-induced Ca^{2+} release suggested an intracellular Ca^{2+} store in HEK293 cells in the absence of caffeine. In contrast, single-channel measurements suggested that RyR1-G4941K rapidly released Ca^{2+} from the intracellular membrane compartment. Neither the potential loss of the FKBP12 subunit from the RyR1 channel complex during purification nor exposure to detergent was found to be responsible for the elevated channel activity in single-channel measurements. The results may be interpreted that the mutant channel underwent a structural change upon removal from the cellular environment.

Previous single-channel studies showed that mutagenesis of the two conserved glycines in the pore-lining S6 pore-lining helix altered RyR function. Substitution of RyR2-Gly-4864 (corresponding to RyR1-Gly-4934) with alanine resulted in no significant changes of RyR2 function, whereas replacement with valine and proline profoundly altered both channel gating and ion permeation (26). Single-channel studies were done using purified RyR2 channel preparations. We reported that replacement of RyR1-Gly-4934 and Gly-4941 with Ala altered RyR1 channel function in single-channel measurements using purified RyR1 preparations (15). A mutation further increasing the side-chain volume at Gly-4934 (G4934V) resulted in loss of function. In contrast, function was maintained when membrane fractions isolated from HEK293 cells were fused with lipid bilayers (18). In this study, loss of function by the G4934D and G4941D mutant channels was seen when proteoliposomes containing the purified mutants or membrane fractions were fused with lipid bilayers.

Aspartic acid has a smaller residue volume than valine (115 Å^3 *versus* 138Å$^{3)}$ (27). This suggested that the introduction of additional negative charges near Asp-4938 and Glu-4942 rendered RyR1-G4934D structurally unstable in HEK293 cells and RyR1-G4941D when removed from the cellular environment.

Modeling the RyR1-G4941K mutation in the open-channel conformation revealed the preferential formation of an intersubunit salt bridge with Asp-4938 (Fig. 10) compared with interaction with Asp-4945. Among the four chains the interaction persists for 34% of the simulation, meaning that on average between one and two salt bridges with Asp-4938 are present at any point in the simulation. Single-channel recordings suggested that the formation of a salt bridge stabilizes the open channel state. In the G4941K/D4945N double mutant, we observed an increase in the G4941K and Asp-4938 interaction in the open-channel conformation and in single-channel measurements a prolonged duration of channel openings. As expected, mutating Asp-4938 to Asn attenuated salt-bridge formation with D4938N. G4941K now showed a preference for intrasubunit salt bridge formation with Asp-4945, and single-

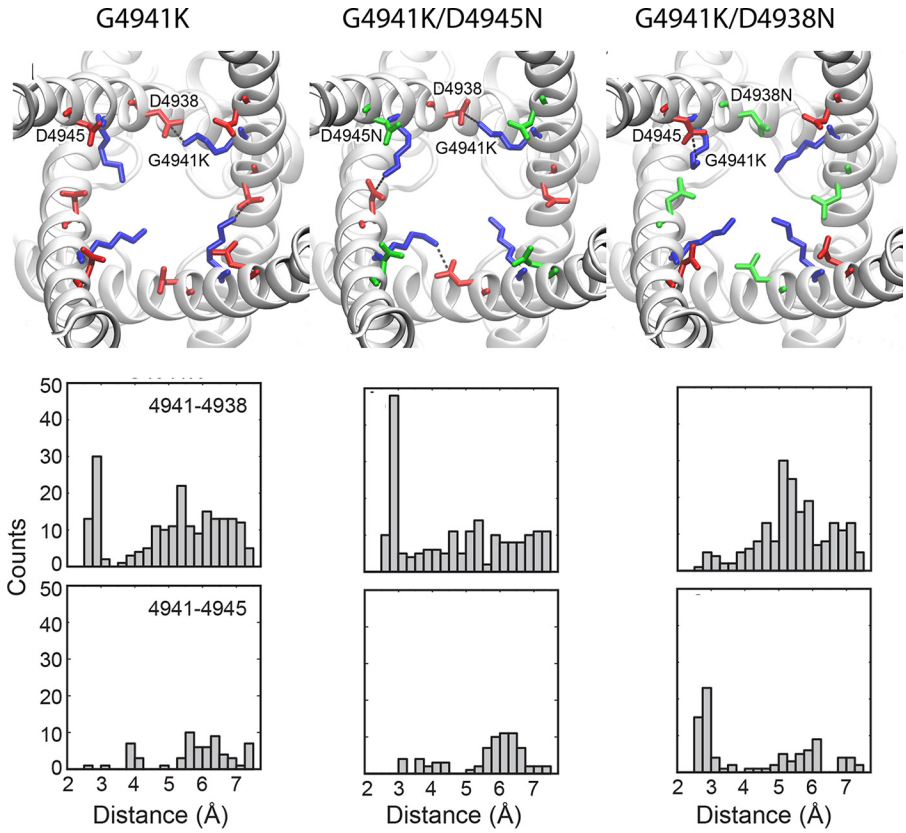

Figure 10. Salt bridges in open mutant channels. *Upper panels* show representative images of salt bridges in G4941K, G4941K/D4945N, and G4941K/D4938N mutant channel structures. Lysine, aspartate, and asparagine are colored *blue, red,* and *green*, respectively. Salt-bridge contacts are shown with *dotted lines*. In the G4941K mutant, G4941K preferentially forms intersubunit salt bridges with Asp-4938 (observed between two of the four chains). An increase in the G4941K–D4938 interaction in the G4941K/D4945N mutant is observed in three of the four chains. In the G4941K/D4938N double mutant, we observe attenuation of the G4941K–D4938N interaction. A small preference of G4941K to form an intrasubunit salt bridge with Asp-4945 is observed in one of four subunits. The *lower panels* show distance distributions for the three mutants. Distances were monitored between the terminal amine groups and the oxygen or nitrogen atoms in the carboxyl or amide side chains. Distances were computed among all four chains for 11 structures sampled from MD simulations of each of the three open-channel RyR1 structures (PDB codes 5t9v, 5tal, and 5ta3). Distances less than 3.5 Å are considered as potential salt bridges. For G4941K, we observe a salt bridge preference between G4941K and Asp-4938. When Asp-4945 is mutated to Asn, we observe an increased preference for the G4941K-Asp-4938 salt bridge. As expected, mutating Asp-4938 to Asn attenuates the salt-bridge formation, and G4941K now shows a preference for Asp-4945.

channel measurements indicated decreased stability of the open-channel in favor of a closed-channel conformation.

Time analysis of the single-channel data is in agreement with these conclusions. The RyR1-G4941K/D4945N double mutant showed a substantial increase in T_o compared with RyR1-G4941K and D4945N, which indicated increased stability of the open-state or a barrier to return to the closed state. In contrast, the G4941K/D4938N double mutation resulted in an elevated T_c compared with G4941K and D4938N, which implies that the closed state was more stable or that there was an additional barrier to opening. As a control, we modeled the open channel conformation of the G4941M mutation and monitored the distances between G4941M and Asp-4938 or Asp-4945 (Fig. 11). We observed closer contacts of G4941M with Asp-4945; however, neither showed significant contacts below the 3.5 Å range required for salt-bridge formation.

Single-channel measurements showed that replacement of glycine with positively charged lysine reduced K^+ conductance and Ca^{2+} selectivity of RyR1-G4941K, G4941K/D4938N, and G4941K/D4945N mutants to a greater extent than G4941M, D4938N, and D4945N mutants. Pore profiles for the open-channel RyR1-G4941K, G4941M, G4941K/D4938N, and G4941K/D4945N mutants are compared with WT in Fig. 12*A*.

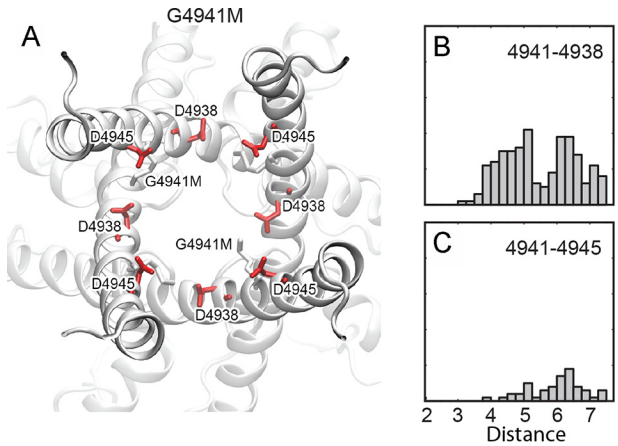

Figure 11. G4941M contacts in the open channel. *A,* as a control the conformations of G4941M are shown with respect to Asp-4938, Asp-4945, and the pore. G4941M is observed to move into an intersubunit pocket that is out of the pore and below Asp-4938 explaining contacts between Asp-4938 and G4941M and the increased pore radius of the G4941M mutation compared with G4941K. The *two right panels* monitor distances between G4941M and Asp-4938 (*B*) or Asp-4945 (*C*). We observe more close contacts between G4941M and Asp-4938 than between G4941M and Asp-4945; however, neither show significant contacts below 3.5 Å (the range expected for salt-bridge formation).

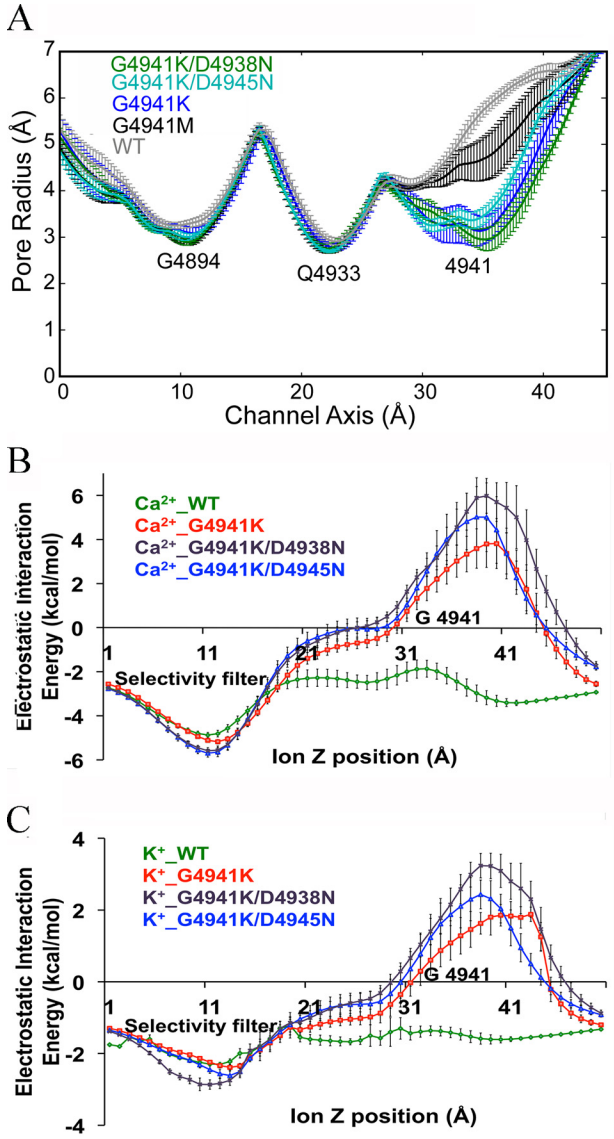

Figure 12. Pore profiles and electrostatic interaction energies for WT and G4941 mutant channels. *A,* Gly-4941 mutations decreased the pore radius from ~5 Å in the WT open channel. The G4941K mutation shows a 3-Å pore radius with a significant amount of fluctuation. Introducing the D4945N mutation to the G4941K mutant preserves the radius of the G4941K mutant but significantly decreases the variance of the radius, likely due to increased preference for intersubunit salt bridges between G4941K and Asp-4938. The G4941K/D4938N double mutant shows a decreased pore radius compared with the G4941K mutant likely due to the formation of less salt bridges and the formation of the G4941K-Asp-4945 intrasubunit salt bridge. A move out of the pore may explain the larger pore radius for methionine compared with lysine in Gly-4941. *B* and *C,* Ca^{2+}– and K^+–protein interaction energies in WT and mutants. Changes in the electrostatics of Ca^{2+} (*B*) and K^+ (*C*) ion passages through the pore in WT-RyR1, G4941K, G4941K/D4938N, and G4941K/D4945N. The interaction energies were estimated by performing APBSmem calculations on 10 structures, which were sampled evenly over the last 5 ns of the respective trajectories. For each of these 10 structures, Ca^{2+} or K^+ were moved through the pore along the channel axis with a step size of 1.0 Å. *Error bars* represent the difference between the means with a 95% confidence interval.

The four mutations had a pore radius comparable with WT at Gly-4894, a site of the selectivity filter, and Gln-4933, the pore constriction site of the open RyRs. In contrast, the G4941K mutation decreased the pore radius from ~5 Å in the WT open channel to ~3 Å. Combining the D4945N mutation with G4941K preserved the radius of RyR1-G4941K but decreased the variance of the radius, likely due to an increased preference for an intersubunit salt bridge between G4941K and Asp-4938. The G4941K/D4938N double mutation resulted in a small decrease in pore radius compared with G4941K, which was likely due to the decreased formation of intersubunit salt bridges. The decreased formation of intersubunit salt bridges caused G4941K to either protrude into the pore or form an intrasubunit salt bridge with Asp-4945, which caused the β, γ, or δ carbons of lysine to protrude into the pore. RyR1-G4941M had a pore radius of ~4.5 Å. A move out of the pore into an intersubunit pocket may explain the larger pore radius for methionine compared with G4941K.

The data of Fig. 12*A* suggest that the flow of ions through the channel will be likely limited at two additional sites (RyR1-Gly-4894 and -Gln-4933). Therefore, the changes in pore size at RyR1-Gly-4941 should not be sufficient to account for the reduced ion conductances of RyR1-G4941K, G4941K/D4938N, and G4941K/D4945N. However, the introduction of positive charges from lysine must be also considered. The change in electrostatics was likely to have had a greater effect on Ca^{2+} carrying a +2 charge than on K^+ carrying a +1 charge. To estimate the electrostatics of the ions within the pore, we calculated the electrostatic Ca^{2+}- and K^+-protein interaction energies using APBSmem software tool (28, 29). Fig. 12, *B* and *C,* shows the interaction energies of the pore residues with Ca^{2+} and K^+ ions as the two ions move through the pore. The results show that the electrostatic interaction energies of WT varied between −5 and −2 kcal/mol for Ca^{2+} and −2.5 and −1 kcal/mol for K^+. A rightward shift from the RyR1-G4941K position was observed for the energy maxima. The negative interaction energies of Ca^{2+} and K^+ are likely primarily due to a favorable interaction with negatively charged amino acid residues (RyR1-Asp-4899 and -Glu-4900) immediately after the GGGIG selectivity motif in the luminal vestibule and negatively charged residues in the cytoplasmic vestibule (Fig. 1*A*). Substitution of glycine in RyR1-G4941K with four positively charged lysine increased interaction energies for Ca^{2+} and K^+ to +6 and +3.3 kcal/mol, respectively. A further moderate increase in the interaction energies was obtained when the negatively charged aspartate residues in Gly-4941/D4938 and Gly-4941/D4945 were replaced with asparagine. Together, the results of Fig. 12 suggest that the introduction of positive charges in G4941K and the further reduction of negative charges in the two double mutants introduced energetic and structural barriers, both of which likely contributed to the reduced ion conductances and selectivities of RyR1-G4941K, G4941K/D4938N, and G4941K/D4945N.

Recent cryo-EM studies identified a binding site for Ca^{2+} at the interface of the RyR1 CSol and C-terminal domains (16). Earlier studies indicated that mutations at other sites affected Ca^{2+}-gated channel activity. Substitution of RyR1-Glu-4032 by alanine and the corresponding amino acid residues in the RyR3 isoform reduced Ca^{2+}-gated channel activity (30, 31). RyR1-Glu-4032 is not part of the Ca^{2+}-binding site but was suggested to stabilize the interaction between two RyR1 regions by H^+ bonding to amide nitrogens (16). Mutations that give rise to central core disease in skeletal muscle exhibit loss of Ca^{2+}-dependent channel activity and Ca^{2+} conductance (32–34). Many

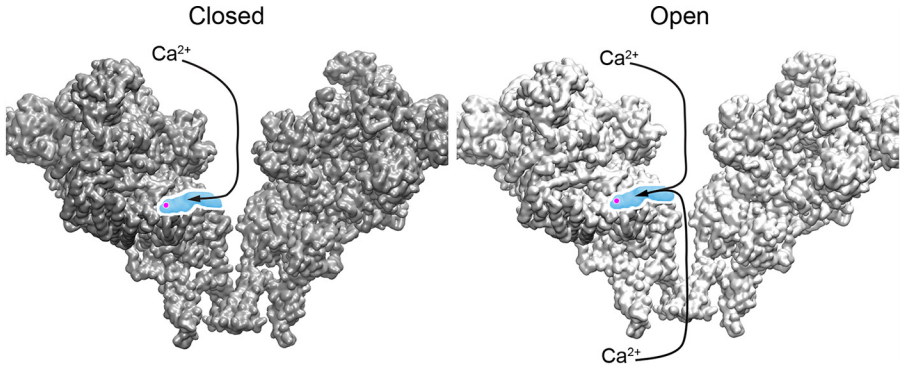

Figure 13. Schematic for cytosolic and luminal Ca^{2+} access to Ca^{2+}-binding site in closed and open RyR1 channels. Two of the four subunits are shown (PDB code 5tal). Closed- and open-channel RyR1 structures are shown in *gray* and *white*, respectively. The position of the Ca^{2+}-binding site is shown in *magenta*. Shown in *blue* is a cutaway of the structure highlighting a cavity through which Ca^{2+} can access the Ca^{2+}-binding site. In the closed-channel RyR1, Ca^{2+} can only access the Ca^{2+}-binding site from the cytosolic side of the channel. However, in the case of an open-channel RyR1 Ca^{2+} can also reach the Ca^{2+}-activation site by approaching from the luminal side of the channel.

of the central core disease mutations are located in the pore-forming region of RyR1. To our knowledge, G4941K mutant has not been associated with a human pathology.

Other sites involved in the regulation of RyR1 by Ca^{2+} include residues in S2 (35), the S4-S5 linker (36, 37), and S6 of the cardiac RyR2 isoform corresponding to RyR1 amino acid residues Gln-4946 to Met-4954 of RyR1 (38). This study extends these findings and shows that sensitivity of RyR1-G4941K to cytosolic and luminal Ca^{2+} increased compared with WT.

Regulation of the RyRs by luminal Ca^{2+} has been attributed to luminal Ca^{2+}-sensing channel sites (22, 39–41), the binding to cytosolic sites following the passage of Ca^{2+} through the open channel (23, 42, 43), or the involvement of Ca^{2+}-sensing sites on both the luminal and cytosolic channel sites (44). To distinguish between luminal and cytosolic Ca^{2+}-regulatory sites, we previously determined the voltage- and Ca^{2+}-dependent regulation of WT-RyR1 (23). As shown in this study, closed WT-RyR1 channels are not activated by luminal Ca^{2+}, and single channels were partially opened by cytosolic ATP in the presence of a low cytosolic Ca^{2+} concentration. Channels were activated by 50 μM luminal Ca^{2+} to a greater extent at negative membrane potentials that favored Ca^{2+} flow through the RyR1 pore than at positive membrane potentials that disfavored passage of Ca^{2+} through RyR1. This suggested that luminal Ca^{2+} bound to cytosolic channel sites following their passage through the open channel. A similar result was obtained when the partially open G4941K mutant channel was recorded at a low cytosolic Ca^{2+} concentration. G4941K was activated to a greater extent by 2 μM luminal Ca^{2+} at negative than positive membrane potentials. These results are best rationalized by luminal Ca^{2+} accessing cytosolic channel sites.

A model consistent with the results of this study suggests that cytosolic Ca^{2+} ions access a recently identified Ca^{2+} activation site located in the cytosolic foot structure of RyR1 (16). The model suggests that cytosolic Ca^{2+} can access the Ca^{2+} activation site when channels are closed or open (Fig. 13). In contrast, luminal Ca^{2+} can access the site in WT only when channels are open. RyR2 channel opening shifts the pore constriction site of Ile-4968 in the closed state to Gln-4864 in the open state (corresponding to Ile-4937 and Gln-4933 in RyR1, respectively) (17). According to the model, luminal Ca^{2+} activates RyR1 when gaining access to the Ca^{2+} activation site following passage through the open-channel RyR1-Gln-4933 restriction site. RyR1-G4941K differs in two respects from WT in its regulation by Ca^{2+}. First, the RyR1-G4941K mutant channel remains open at low cytosolic Ca^{2+} concentrations; second, it exhibits an increased sensitivity to activation by cytosolic and luminal Ca^{2+} compared with WT. Our results suggest that luminal Ca^{2+} accesses Ca^{2+} activation sites as they pass through the pore rather than traveling to openings that lie outside the pore.

Experimental procedures

Materials

[^{3}H]Ryanodine was obtained from PerkinElmer Life Sciences; protease and phosphatase inhibitors were from Sigma, and phospholipids were from Avanti Polar Lipids.

Preparation of wildtype and mutant channels

RyR1 mutations G4934D, G4934K, G4941D, and G4941K were introduced by *Pfu* polymerase-based chain reaction using mutagenic oligonucleotides and the QuikChange II site-directed mutagenesis kit (Stratagene, La Jolla, CA) (45). RyR1-G4941M, G4941K/D4938N, and G4941K/D4945N were prepared using a gene synthesis method and a proprietary protocol (Genewiz, Inc., South Plainfield, NJ). WT-RyR1 and mutants were transiently expressed in HEK293 cells using FuGENE 6 (Roche Applied Sciences) or jetPRIME (Polyplus, New York) according to the manufacturers' instructions. Cells were maintained in DMEM/F-12 (1:1) medium containing 10% fetal bovine serum at 37 °C and 5% CO_2 and plated the day before transfection. Following transfection, cells were maintained at 35 or 37 °C and harvested ~70 h after transfection. Crude membrane isolates (45) and proteoliposomes containing purified WT or mutant RyR1 channels were prepared as described (20).

Cellular Ca^{2+} release

Stored Ca^{2+} release was determined as described (46). Briefly, HEK293 cells were grown on glass coverslips, and Ca^{2+} transients were monitored with the fluorescence Ca^{2+} indicator Fluo-4. The addition of ~8 mM caffeine induced cellular Ca^{2+} release. Individ-

ual cells were monitored using the EasyRatioPro algorithm (Photon Technology International, Lawrenceville, NJ).

SDS-PAGE and immunoblot analyses

Proteins in crude membrane fractions (20 μg of protein/lane) were separated using 3–12% gradient SDS-PAGE, transferred overnight to nitrocellulose membranes (37), and probed with primary rabbit anti-RyR1 polyclonal antibody 6425 prepared by ΨProSci against RyR1 sequence FIKGLDSFSGKPRGSG. Immunoblots were developed using enhanced chemiluminescence and quantified using the Bio-Rad ChemiDoc MP Imaging System and ImageQuantTL analysis software.

[^{3}H]Ryanodine binding

Ryanodine binds with high specificity to RyR1 and is widely used to probe RyR activity and content (19). [^{3}H]Ryanodine binding was measured by incubating crude membrane isolates for 4–5 h at 24 °C with a near-saturating concentration of 20 nM [^{3}H]ryanodine in 20 mM imidazole, pH 7.0, 0.6 M KCl, protease inhibitors, 1 mM oxidized glutathione (GSSG), and 0.1 mM Ca^{2+}. Non-specific binding was determined using a 100-fold excess of unlabeled ryanodine. Aliquots of samples were diluted 9-fold with ice-cold water and placed on Whatman GF/B filters saturated with 2% polyethyleneimine. Filters were washed with ice-cold 0.1 M KCl, 1 mM imidazole, pH 7.0. Radioactivity remaining on the filters was determined by liquid scintillation counting to obtain bound [^{3}H]ryanodine.

Single-channel recordings

Single-channel measurements were performed using planar lipid bilayers (14). Unless otherwise indicated, proteoliposomes containing purified recombinant RyR1s were added to the *cis* (cytosolic) chamber of a bilayer apparatus containing 0.25 M KCl in the *cis* chamber and 20 mM KCl in the *trans* (SR luminal) chamber in 20 mM KHEPES, pH 7.4, and 2 μM Ca^{2+}. After the appearance of channel activity, the *trans* KCl concentration was increased to 0.25 M KCl. A strong dependence of WT channel activity on *cis* Ca^{2+} concentration indicated that the cytosolic region faced the *cis* chamber of the bilayer. The *trans* side of the bilayer was defined as ground. Electrical signals were filtered at 2 kHz (0.5 kHz for Ca^{2+} currents at 0 mV), digitized at 10 kHz, and analyzed at 50% threshold setting (14). Data acquisition and analysis of 2-min recordings were performed using a commercially available software package (pClamp, Axon Instruments). Single-channel activities were also recorded in symmetrical 0.25 M KCl solution with 10 mM Ca^{2+} on the *trans* side, and the reversal potential (E_{rev}) was measured to determine permeability ratios. The permeability ratio of Ca^{2+} *versus* K^+ (P_{Ca}/P_K) was calculated using a modified form of the Goldman-Hodgkin-Katz Equation 1,

$$E_{rev} = -\frac{RT}{F}\ln\left\{[K]^{\frac{1}{2}} \times \left([K] + 4\frac{P_{Ca}}{P_K}[Ca]\right)^{-\frac{1}{2}}\right\} \qquad \text{(Eq. 1)}$$

Computational methods

To model the effects of the mutations, *in silico* mutations were performed for each of the three open-channel cryo-EM structures (PDB codes 5tal, 5t9v, and 5ta3). Amino acid substitutions were performed using Eris (47, 48) followed by side-chain optimization in GROMACS 4.6.1 (49). Starting structures from Eris were obtained from 40 independent Monte-Carlo simulations with 20 steps each. The lowest energy structure among the 40 structures was selected as the starting point for GROMACS simulations. Each system was solvated using the TIP3P water model. Simulations were performed using the CHARMM36 force field (50, 51). The systems were equilibrated with 10,000 steps of steepest descent energy minimization followed by 200 ps of constant volume MD simulation performed at 310 K. Simulations were performed using a time step of 2 fs with all bonds constrained using the LINCS algorithm (52). Particle mesh Ewald was used for long-range electrostatic interactions. A 10-Å cutoff was used for non-bonded interactions. For production runs, 10 ns of MD simulations were performed at constant temperature and pressure of 310 K and 1 atm followed by 4 ns of annealing. For annealing simulations, pressure was held constant at 1 atm, whereas temperature was linearly decreased from 310 to 200 K. A 10,000 kJ/(mol·nm) potential was applied to fix the backbone atoms throughout the simulations and prevent large structural arrangements in the absence of the membrane. For analysis, 10 structures sampled evenly over the last 5 ns of the simulation were extracted. Pore profiles were calculated using the HOLE program (53). Data are the mean and standard error among 30 pore profiles computed from the sampled structures.

The Adaptive Poisson-Boltzmann Solver (APBS) as applied in APBSmem (28) was used to examine the electrostatics of Ca^{2+} and K^+ ion passage through the pore. APBSmem estimates the protein-ion electrostatic interaction energy by subtracting the energies of the membrane-embedded protein without the ion and the energy of the ion in bulk water from the total energy of the protein-ion assembly embedded in the lipid bilayer. For analysis, 10 WT and mutant structures sampled evenly over the last 5 ns of the respective simulations were extracted. Two focusing layers with a grid length of 90 Å and a total of 97 grid points in the *x*, *y*, and *z* dimensions were employed. Ion concentrations were set at 0.1 M, both for Ca^{2+} and K^+; the temperature was 298 K, and non-linear Poisson-Boltzmann method was engaged in Adaptive Poisson-Boltzmann Solver (29). To omit the membrane from the pore region, the upper and lower exclusions were set at 16 Å. Based on previously reported calculations of Ca^{2+} solvation energy profile of the TRPV1 receptor (54), membrane thickness was 42.5 Å, and headgroup thickness was 7 Å. During the calculation, the dielectric constant for protein and membrane was set at 2.0, and the dielectric constant for headgroups and solvent was set at 80.0. The ion step size was 1.0 Å along the channel axis and the ionic radius used for Ca^{2+} and K^+ were 1.03 and 1.41 Å, respectively.

Biochemical assays and data analysis

Free Ca^{2+} concentrations were determined by adding varying amounts of Ca^{2+} to 1 mM EGTA solutions. Free Ca^{2+} concentrations were measured using a Ca^{2+}-selective electrode. Differences between samples were analyzed using Student's *t*

test or analysis of variance followed by Tukey's test, where $p < 0.05$ was considered significant.

Author contributions—L. X., D. D. M., N. V. D., and G. M. designed the experiments; L. X., D. D. M., V. R. C., Y. W., and D. A. P. performed the experiments, and D. D. M. and G. M. wrote the paper. All authors reviewed the results and approved the final version of the manuscript.

References

1. Franzini-Armstrong, C., and Protasi, F. (1997) Ryanodine receptors of striated muscles: a complex channel capable of multiple interactions. *Physiol. Rev.* **77,** 699–729 CrossRef Medline
2. Fill, M., and Copello, J. A. (2002) Ryanodine receptor calcium release channels. *Physiol. Rev.* **82,** 893–922 CrossRef Medline
3. Meissner, G. (2002) Regulation of mammalian ryanodine receptors. *Front. Biosci.* **7,** d2072–d2080 Medline
4. Meissner, G. (1994) Ryanodine receptor/Ca^{2+} release channels and their regulation by endogenous effectors. *Annu. Rev. Physiol.* **56,** 485–508 CrossRef Medline
5. Hamilton, S. L., and Serysheva, I. I. (2009) Ryanodine receptor structure: progress and challenges. *J. Biol. Chem.* **284,** 4047–4051 CrossRef Medline
6. Lanner, J. T., Georgiou, D. K., Joshi, A. D., and Hamilton, S. L. (2010) Ryanodine receptors: structure, expression, molecular details, and function in calcium release. *Cold Spring Harb. Perspect. Biol.* **2,** a003996 Medline
7. Yan, Z., Bai, X., Yan, C., Wu, J., Li, Z., Xie, T., Peng, W., Yin, C. C., Li, X., Scheres, S. H., Shi, Y., and Yan, N. (2015) Structure of the rabbit ryanodine receptor RyR1 at near-atomic resolution. *Nature* **517,** 50–55 Medline
8. Gao, L., Balshaw, D., Xu, L., Tripathy, A., Xin, C., and Meissner, G. (2000) Evidence for a role of the lumenal M3-M4 loop in skeletal muscle Ca^{2+} release channel (ryanodine receptor) activity and conductance. *Biophys. J.* **79,** 828–840 CrossRef Medline
9. Efremov, R. G., Leitner, A., Aebersold, R., and Raunser, S. (2015) Architecture and conformational switch mechanism of the ryanodine receptor. *Nature* **517,** 39–43 Medline
10. Ludtke, S. J., Serysheva, I. I., Hamilton, S. L., and Chiu, W. (2005) The pore structure of the closed RyR1 channel. *Structure* **13,** 1203–1211 CrossRef Medline
11. Samso, M., Feng, W., Pessah, I. N., and Allen, P. D. (2009) Coordinated movement of cytoplasmic and transmembrane domains of RyR1 upon gating. *PLoS Biol.* **7,** e85 CrossRef Medline
12. Zalk, R., Clarke, O. B., des Georges, A., Grassucci, R. A., Reiken, S., Mancia, F., Hendrickson, W. A., Frank, J., and Marks, A. R. (2015) Structure of a mammalian ryanodine receptor. *Nature* **517,** 44–49 Medline
13. Wang, Y., Xu, L., Pasek, D. A., Gillespie, D., and Meissner, G. (2005) Probing the role of negatively charged amino acid residues in ion permeation of skeletal muscle ryanodine receptor. *Biophys. J.* **89,** 256–265 CrossRef Medline
14. Xu, L., Wang, Y., Gillespie, D., and Meissner, G. (2006) Two rings of negative charges in the cytosolic vestibule of type-1 ryanodine receptor modulate ion fluxes. *Biophys. J.* **90,** 443–453 CrossRef Medline
15. Mei, Y., Xu, L., Mowrey, D. D., Mendez Giraldez, R., Wang, Y., Pasek, D. A., Dokholyan, N. V., and Meissner, G. (2015) Channel gating dependence on pore-lining helix glycine residues in skeletal muscle ryanodine receptor. *J. Biol. Chem.* **290,** 17535–17545 CrossRef Medline
16. des Georges, A., Clarke, O. B., Zalk, R., Yuan, Q., Condon, K. J., Grassucci, R. A., Hendrickson, W. A., Marks, A. R., and Frank, J. (2016) Structural basis for gating and activation of RyR1. *Cell* **167,** 145–157 CrossRef Medline
17. Peng, W., Shen, H., Wu, J., Guo, W., Pan, X., Wang, R., Chen, S. R., and Yan, N. (2016) Structural basis for the gating mechanism of the type 2 ryanodine receptor RyR2. *Science* **354,** aah5324 Medline
18. Mowrey, D. D., Xu, L., Mei, Y., Pasek, D. A., Meissner, G., and Dokholyan, N. V. (2017) Ion-pulling simulations provide insights into the mechanisms of channel opening of the skeletal muscle ryanodine receptor. *J. Biol. Chem.* **292,** 12947–12958 CrossRef Medline
19. Sutko, J. L., Airey, J. A., Welch, W., and Ruest, L. (1997) The pharmacology of ryanodine and related compounds. *Pharmacol. Rev.* **49,** 53–98 Medline
20. Lee, H. B., Xu, L., and Meissner, G. (1994) Reconstitution of the skeletal muscle ryanodine receptor-Ca^{2+} release channel protein complex into proteoliposomes. *J. Biol. Chem.* **269,** 13305–13312 Medline
21. Meissner, G., Darling, E., and Eveleth, J. (1986) Kinetics of rapid Ca^{2+} release by sarcoplasmic reticulum. Effects of Ca^{2+}, Mg^{2+}, and adenine nucleotides. *Biochemistry* **25,** 236–244 CrossRef Medline
22. Sitsapesan, R., and Williams, A. J. (1995) The gating of the sheep skeletal sarcoplasmic reticulum Ca^{2+}-release channel is regulated by luminal Ca^{2+}. *J. Membr. Biol.* **146,** 133–144 Medline
23. Tripathy, A., and Meissner, G. (1996) Sarcoplasmic reticulum lumenal Ca^{2+} has access to cytosolic activation and inactivation sites of skeletal muscle Ca^{2+} release channel. *Biophys. J.* **70,** 2600–2615 CrossRef Medline
24. Ahern, G. P., Junankar, P. R., and Dulhunty, A. F. (1994) Single channel activity of the ryanodine receptor calcium release channel is modulated by FK-506. *FEBS Lett.* **352,** 369–374 CrossRef Medline
25. Brillantes, A. B., Ondrias, K., Scott, A., Kobrinsky, E., Ondriasová, E., Moschella, M. C., Jayaraman, T., Landers, M., Ehrlich, B. E., and Marks, A. R. (1994) Stabilization of calcium release channel (ryanodine receptor) function by FK506-binding protein. *Cell* **77,** 513–523 CrossRef Medline
26. Euden, J., Mason, S. A., Viero, C., Thomas, N. L., and Williams, A. J. (2013) Investigations of the contribution of a putative glycine hinge to ryanodine receptor channel gating. *J. Biol. Chem.* **288,** 16671–16679 CrossRef Medline
27. Tsai, J., Taylor, R., Chothia, C., and Gerstein, M. (1999) The packing density in proteins: standard radii and volumes. *J. Mol. Biol.* **290,** 253–266 CrossRef Medline
28. Callenberg, K. M., Choudhary, O. P., de Forest, G. L., Gohara, D. W., Baker, N. A., and Grabe, M. (2010) APBSmem: a graphical interface for electrostatic calculations at the membrane. *PLoS One* **5,** e12722 CrossRef Medline
29. Baker, N. A., Sept, D., Joseph, S., Holst, M. J., and McCammon, J. A. (2001) Electrostatics of nanosystems: application to microtubules and the ribosome. *Proc. Natl. Acad. Sci. U.S.A.* **98,** 10037–10041 CrossRef Medline
30. Chen, S. R., Ebisawa, K., Li, X., and Zhang, L. (1998) Molecular identification of the ryanodine receptor Ca^{2+} sensor. *J. Biol. Chem.* **273,** 14675–14678 CrossRef Medline
31. Du, G. G., and MacLennan, D. H. (1998) Functional consequences of mutations of conserved, polar amino acids in transmembrane sequences of the Ca^{2+} release channel (ryanodine receptor) of rabbit skeletal muscle sarcoplasmic reticulum. *J. Biol. Chem.* **273,** 31867–31872 CrossRef Medline
32. Dirksen, R. T., and Avila, G. (2002) Altered ryanodine receptor function in central core disease: leaky or uncoupled Ca^{2+} release channels? *Trends Cardiovasc. Med.* **12,** 189–197 CrossRef Medline
33. Xu, L., Wang, Y., Yamaguchi, N., Pasek, D. A., and Meissner, G. (2008) Single channel properties of heterotetrameric mutant RyR1 ion channels linked to core myopathies. *J. Biol. Chem.* **283,** 6321–6329 CrossRef Medline
34. McCarthy, T. V., Quane, K. A., and Lynch, P. J. (2000) Ryanodine receptor mutations in malignant hyperthermia and central core disease. *Hum. Mutat.* **15,** 410–417 CrossRef Medline
35. Gomez, A. C., and Yamaguchi, N. (2014) Two regions of the ryanodine receptor calcium channel are involved in Ca^{2+}-dependent inactivation. *Biochemistry* **53,** 1373–1379 CrossRef Medline
36. Murayama, T., Kurebayashi, N., Oba, T., Oyamada, H., Oguchi, K., Sakurai, T., and Ogawa, Y. (2011) Role of amino-terminal half of the S4-S5 linker in type 1 ryanodine receptor (RyR1) channel gating. *J. Biol. Chem.* **286,** 35571–35577 CrossRef Medline
37. Ramachandran, S., Chakraborty, A., Xu, L., Mei, Y., Samsó, M., Dokholyan, N. V., and Meissner, G. (2013) Structural determinants of skeletal muscle ryanodine receptor gating. *J. Biol. Chem.* **288,** 6154–6165 CrossRef Medline
38. Sun, B., Guo, W., Tian, X., Yao, J., Zhang, L., Wang, R., and Chen, S. R. (2016) The cytoplasmic region of inner helix S6 is an important determi-

nant of cardiac ryanodine receptor channel gating. *J. Biol. Chem.* **291,** 26024–26034 CrossRef Medline
39. Gaburjakova, J., and Gaburjakova, M. (2016) Cardiac ryanodine receptor: selectivity for alkaline earth metal cations points to the EF-hand nature of luminal binding sites. *Bioelectrochemistry* **109,** 49–56 CrossRef Medline
40. Györke, I., and Györke, S. (1998) Regulation of the cardiac ryanodine receptor channel by luminal Ca^{2+} involves luminal Ca^{2+} sensing sites. *Biophys. J.* **75,** 2801–2810 CrossRef Medline
41. Gaburjakova, J., and Gaburjakova, M. (2006) Comparison of the effects exerted by luminal Ca^{2+} on the sensitivity of the cardiac ryanodine receptor to caffeine and cytosolic Ca^{2+}. *J. Membr. Biol.* **212,** 17–28 CrossRef Medline
42. Uehara, A., Murayama, T., Yasukochi, M., Fill, M., Horie, M., Okamoto, T., Matsuura, Y., Uehara, K., Fujimoto, T., Sakurai, T., and Kurebayashi, N. (2017) Extensive Ca^{2+} leak through K4750Q cardiac ryanodine receptors caused by cytosolic and luminal Ca^{2+} hypersensitivity. *J. Gen. Physiol.* **149,** 199–218 CrossRef Medline
43. Herrmann-Frank, A., and Lehmann-Horn, F. (1996) Regulation of the purified Ca^{2+} release channel/ryanodine receptor complex of skeletal muscle sarcoplasmic reticulum by luminal calcium. *Pflugers Arch.* **432,** 155–157 CrossRef Medline
44. Laver, D. R. (2007) Ca^{2+} stores regulate ryanodine receptor Ca^{2+} release channels via luminal and cytosolic Ca^{2+} sites. *Biophys. J.* **92,** 3541–3555 CrossRef Medline
45. Gao, L., Tripathy, A., Lu, X., and Meissner, G. (1997) Evidence for a role of C-terminal amino acid residues in skeletal muscle Ca^{2+} release channel (ryanodine receptor) function. *FEBS Lett.* **412,** 223–226 CrossRef Medline
46. Wang, Y., Xu, L., Duan, H., Pasek, D. A., Eu, J. P., and Meissner, G. (2006) Knocking down type 2 but not type 1 calsequestrin reduces calcium sequestration and release in C2C12 skeletal muscle myotubes. *J. Biol. Chem.* **281,** 15572–15581 CrossRef Medline
47. Yin, S., Ding, F., and Dokholyan, N. V. (2007) Modeling backbone flexibility improves protein stability estimation. *Structure* **15,** 1567–1576 CrossRef Medline
48. Yin, S., Ding, F., and Dokholyan, N. V. (2007) Eris: an automated estimator of protein stability. *Nat. Methods* **4,** 466–467 CrossRef Medline
49. Hess, B., Kutzner, C., van der Spoel, D., and Lindahl, E. (2008) GROMACS 4: algorithms for highly efficient, load-balanced, and scalable molecular simulation. *J. Chem. Theory Comput.* **4,** 435–447 CrossRef Medline
50. Best, R. B., Zhu, X., Shim, J., Lopes, P. E., Mittal, J., Feig, M., and Mackerell, A. D., Jr. (2012) Optimization of the additive CHARMM all-atom protein force field targeting improved sampling of the backbone ϕ, ψ, and side-chain χ^1 and χ^2 dihedral angles. *J. Chem. Theory Comput.* **8,** 3257–3273 CrossRef Medline
51. Klauda, J. B., Monje, V., Kim, T., and Im, W. (2012) Improving the CHARMM force field for polyunsaturated fatty acid chains. *J. Phys. Chem. B* **116,** 9424–9431 CrossRef Medline
52. Hess, B. (2008) P-LINCS: a parallel linear constraint solver for molecular simulation. *J. Chem. Theory Comput.* **4,** 116–122 CrossRef Medline
53. Smart, O. S., Neduvelil, J. G., Wang, X., Wallace, B. A., and Sansom, M. S. (1996) HOLE: a program for the analysis of the pore dimensions of ion channel structural models. *J. Mol. Graph.* **14,** 354–360 Medline
54. Marcoline, F. V., Bethel, N., Guerriero, C. J., Brodsky, J. L., and Grabe, M. (2015) Membrane protein properties revealed through data-rich electrostatics calculations. *Structure* **23,** 1526–1537 CrossRef Medline

G4941K substitution in the pore-lining S6 helix of the skeletal muscle ryanodine receptor increases RyR1 sensitivity to cytosolic and luminal Ca^{2+}

Le Xu, David D. Mowrey, Venkat R. Chirasani, Ying Wang, Daniel A. Pasek, Nikolay V. Dokholyan and Gerhard Meissner

J. Biol. Chem. 2018, 293:2015-2028.
doi: 10.1074/jbc.M117.803247 originally published online December 18, 2017